ISSN 1066-3622, Radiochemistry, 2020, Vol. 62, No. 3, pp. 335–346. © Pleiades Publishing, Inc., 2020.

Adsorption of ^{141}Ce(III), ^{160}Tb(III), and ^{169}Yb(III) on the Synthesized Inorganic Ion Exchanger, Zirconium Titanium Phosphate

F. H. El-Sweify[a,*], A. A. Abdel-Fattah[a], M. A. Ghamry[a], S. M. Aly[a], and M. F. El-Shahat[b]

[a] *Nuclear Chemistry Department, Radioisotopes Production and Radiation Sources Division, Hot Laboratories Center, Atomic Energy Authority, Inshas, Cairo, 13759 Egypt*
[b] *Chemistry Department, Faculty of Science, Ain Shames University, Cairo, 11566 Egypt*
**e-mail: felsweify@hotmail.com*

Received April 17, 2019; revised May 13, 2019; accepted May 20, 2019

Abstract—Samples of zirconium titanium phosphate inorganic ion exchangers with different Zr : Ti molar ratios were synthesized. The samples were characterized using FT-IR spectroscopy, X-ray diffraction, scanning electron microscopy, and pore size analysis. The adsorption behavior of lanthanide isotopes ^{141}Ce(III), ^{160}Tb(III), and ^{169}Yb(III) was studied in batch experiments. The influence of the *V*/*m* ratio (mL g^{-1}), solution pH, contact time, particle size, metal ion concentration, and temperature on the adsorption kinetics was studied. The changes in the Gibbs free energy, enthalpy, and entropy were calculated. The adsorption isotherms and kinetics were analyzed using different models. The adsorption was found to follow the Langmuir isotherm better than the Freundlich isotherm. The pseudo-second-order kinetic model fits the adsorption data.

Keywords: adsorption, zirconium titanium phosphate, cerium-141, terbium-160, ytterbium-169

DOI: 10.1134/S1066362220030066

INTRODUCTION

Rare earth (RE) elements, especially lanthanides, have increasing unique applications in numerous fields. These include nuclear technologies (e.g., fabrication of control rods), use in various technologies, e.g., as catalysts in petroleum industry, production of low-alloy steels for plates and pipes to enhance their strength and work ability, production of lighter flints using mixed lanthanide–Mg-based alloys, in ceramics and glass for different purposes, in construction of permanent magnets, also in electronics, superconductor production, and medicine [1–4]. The lanthanides (Ce–Lu) resemble each other markedly in their chemical behavior [1].

The +3 oxidation state is characteristic of all the lanthanides both in solid compounds and in solutions in water and other solvents. A few solid compounds with the +4 state have been reported [1, 5], but only Ce^{4+} shows some stability in aqueous solutions and has some importance in aqueous chemistry. Eu^{2+} and Yb^{2+} also show some stability [5, 6].

The atomic radii decrease from lanthanum to lutetium (lanthanide contraction), which is due to imperfect shielding of one 4*f* electron by another 4*f* electron [1, 5]. As the nuclear charge and thus the number of 4*f* electrons increase, the imperfect shielding accused by directed nature of 4*f* orbitals causes each 4*f* electron to experience an added electrostatic attraction by the nucleus, resulting in a decrease in the size of the entire 4*f* arrangement and therefore in the sizes of atoms and ions with increasing atomic number [5].

The aqueous lanthanide(III) and Y(III) cations are believed to have the H_2O coordination number of 9 up to approximately the middle of the series at which point the number changes to 8 [6].

In this work, we studied the sorption of Ce, Tb, and Yb ionic species from aqueous solutions onto the synthesized inorganic ion exchangers and the influence of various factors on their behavior. These elements were chosen because they may have, in addition to the trivalent state, also the tetravalent (Ce, Tb) and divalent (Yb) state depending on the conditions.

EXPERIMENTAL

Chemicals. All the chemicals used were of analytical grade. Zirconyl chloride ($ZrOCl_2 \cdot 8H_2O$) was a product of Merck (Germany), titanium tetrachloride was a product of BDH (the United Kingdom), and phosphoric acid was a product of Pekings reagent (the United Kingdom).

Radioisotopes. The radioisotopes ^{141}Ce, ^{160}Tb, and ^{169}Yb were used to trace the corresponding elements; the concentration of these elements was determined by γ-ray radiometry. ^{141}Ce ($T_{1/2}$ = 32.5 days), ^{160}Tb ($T_{1/2}$ = 72.1 days), and ^{169}Yb ($T_{1/2}$ = 32.9 days) were produced by irradiating the corresponding salts in the Egyptian reactor ET-RR-2 at Inshas. 0.5-g portions of $CeCl_3 \cdot 7H_2O$, $TbCl_3 \cdot 6H_2O$, and Yb_2O_3 (Merck, Germany) were used for preparing the corresponding radioactive isotopes. Stock solutions of these elements were prepared in HCl solutions. These radioisotopes were produced by the following nuclear reactions:

$$^{140}Ce\ (a = 88.5\%) \xrightarrow[(\sigma = 0.57b)]{(n,\gamma)} {}^{141}Ce \xrightarrow[T_{1/2} = 32.5d]{\beta^-,\gamma\ (145\ keV)} {}^{141}Pr\ \text{Stable} \quad (I)$$

$$^{159}Tb\ (a = 100\%) \xrightarrow[(\sigma = 25.5b)]{(n,\gamma)} {}^{160}Tb \xrightarrow[T_{1/2} = 72.1d]{\beta^-,\gamma\ (878,299\ keV)} {}^{160}Dy\ \text{Stable} \quad (II)$$

$$^{168}Yb\ (a = 0.14\%) \xrightarrow[(\sigma = 3470b)]{n,\gamma\ (878\ keV)} {}^{169}Yb \xrightarrow[T_{1/2} = 30.7d]{\varepsilon,\gamma\ (198\ keV)} {}^{169}Tm\ \text{Stable} \quad (III)$$

where a is the isotopic abundance (%), σ is the cross section for the (n, γ) reaction (barn), and $T_{1/2}$ is the half-life of the radioactive isotope [7]. These isotopes ^{141}Ce, ^{160}Tb, and ^{169}Yb were chosen because of their suitable nuclear properties for the measurements such as half-life, γ-ray energy (keV), and intensity (%).

All the radioisotopes were assayed γ-radiometrically using an 8192-multichannel analyzer with a hyperpure Ge detector with a resolution of 1.8 keV (FWHM) at 1332.5 keV and 30% efficiency relative to a NaI(Tl) detector, connected to an IBM computer. The γ-ray peaks of the relevant radionuclides were analyzed at their characteristic energies: 145, 878, and 198 keV for ^{141}Ce, ^{160}Tb, and ^{169}Yb, respectively. In some experiments, these radioisotopes were analyzed in the presence of each other in solution without any resolution difficulties.

Every measurement was repeated three times; the standard deviation (±SD) and the relative standard deviation (RSD %) in each case were determined using the following equations:

$$SD = \pm\sqrt{\frac{1}{N-1}\sum_{i=1}^{N}(X_i - X)^2} \quad (1)$$

and

$$RSD = \frac{SD}{x_i} \times 100, \quad (2)$$

where x_i is the mean value and x is the radioactivity in each case.

Synthesis of zirconium titanium phosphate. Zirconium titanium phosphate (ZTP) was synthesized by the procedure described by Marei and Shakshooki [8] as well as in the previous work [9, 10]. Equimolar quantities of zirconyl chloride ($ZrOCl_2 \cdot 8H_2O$) and titanium chloride (pure $TiCl_4$) were individually dissolved in 4 M HCl. Definite volumes of these two solutions, calculated to give Zr : Ti molar ratios of 5 : 95, 25 : 75, and 95 : 5, were mixed and stirred for 1 h. To the clear solution, 12% phosphoric acid in 4 M HCl was added slowly with stirring at a constant temperature of 25 ± 1°C until the precipitation was complete. The formed fine white precipitates of zirconium titanium phosphate were left to settle for 48 h before being filtered and washed with 4 M HCl. The precipitate was then washed with double-distilled water until pH of the wash water became about 3. The formed zirconium titanium phosphate samples were redried at 50°C, ground, sieved to the desired mesh size using standard sieves (F. Kurt Retsch, Germany), and stored in a desiccator before use. The synthesized samples were analyzed by FT-IR spectrometry with a Bomem Michelson FT-IR spectrometer (MB-series 157, Canada). The morphology and grain size of the ZTP samples were determined with by scanning electron microscopy (SEM) (JSM-6510A

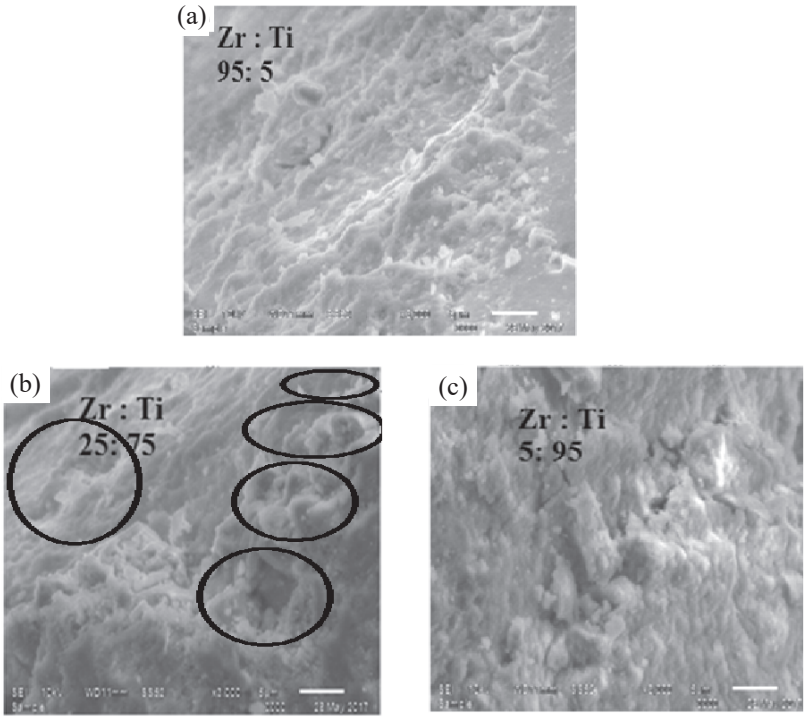

Fig. 1. SEM images of the ZTP samples. Zr : Ti molar ratio: (a) 95 : 5, (b) 25 : 75, and (c) 5 : 95.

model, Jeol, Japan) with the primary electron beam energy ranging from 5 to 30 keV. X-ray diffraction analysis were carried out using a Philips X-Ray diffractometer, model PW 1890, with a nickel filter and a CuK_α X-radiation tube. The total pore area, average pore diameter, and porosity of the ZTP samples with the Zr : Ti molar ratios of 95 : 5, 25 : 75 and 5 : 59 (particle size >160 μm) were deteremined with a Pore Sizer 9320 device (Micromeritics, the United States).

Batch sorption experiments. The distribution coefficient and uptake percentage values for the adsorption of ^{141}Ce(III), ^{160}Tb(III), and ^{169}Yb(III) onto ZTP samples were determined in batch experiments. 5.0-mL aliquots of a solution containing the desired radioactive isotopes were equilibrated with 0.05 g of the ZTP ion exchanger (except experiments on studying the effect of *V*/*m*, when different weighed portions of ZTP were taken). The mixtures were shaken mechanically at 30 ± 1°C for a predetermined period using a thermostat shaker. After that, aliquots of the aqueous solution were withdrawn and assayed radiometrically to determine the running value of the distribution coefficient K_d (mL g^{-1}) and the percentage uptake (%):

$$K_d = \frac{A_0 - A}{A} \times \frac{V}{m} \text{ (mL g}^{-1}\text{)}, \quad (3)$$

$$\text{Uptake} = \frac{A_0 - A}{A} \times 100, \quad (4)$$

where A_0 and A are the areas under the γ-ray peaks of the given radionuclide before and after contacting time with the ion exchanger, respectively; V, aqueous phase volume (mL); and m, ion exchanger weight (g).

RESULTS AND DISCUSSION

Scanning electron microscopy. The SEM images of the three synthesized ZTP samples are shown in Fig. 1. The surface in Figs. 1a and 1c is smoother and more continuous than in Fig. 1b; this may be attributed to the difference in the size of the Zr(IV) and Ti(IV) ions. The ionic radii of 6-coordinated Zr(IV) and Ti(IV) are 72 and 60.5 pm, respectively [1]. In the case of ZTP with the Zr : Ti molar ratio of 95 : 5 or 5 : 95, the amount of the minor component is small relative to the major component, which may lead to the formation of a more homogeneous material, compared to ZTP with Zr : Ti = 25 : 75, where the probable random arrangement of the ions of different radii may lead to lower homogeneity.

The results of measuring the total pore area, average pore diameter, and porosity are given in Table 1.

Table 1. Some properties of Ce, Tb, and Yb

Property [1]	Ce	Tb	Yb
Atomic number	58	65	70
Oxidation state:	III, IV	III, IV	II, III
Ionic radius (coordination number 6), pm	102 (III), 87 (IV)	92.3 (III), 76 (IV)	102 (II), 85.8 (III)
Hydrolysis [6]	IV: $Ce(OH)_2^{2+}$ (pH < 0) ; III: Ce_{aq}^{3+} (pH ≤ 7.1), $Ce(OH)_{3(s)}$ (pH > 7.1)	Tb_{aq}^{3+} (pH ≤ 6.3), $Tb(OH)_{3(s)}$ (pH > 6.3)	Yb_{aq}^{3+} (pH ≤ 5.6), $Yb(OH)_{3(s)}$ (pH > 5.6)

FT-IR spectra. The FT-IR spectra of the synthesized ZTP samples are shown in Fig. 2. A broad strong band at 3460–3410 cm^{-1} appears in the spectra. This band is attributed to stretching vibrations of water molecules involved in intermolecular hydrogen bonds. A medium-intensity sharp peak in the range 1640–1630 cm^{-1} can be assigned to OH bending vibrations. A strong peak in the range 1100–1000 cm^{-1} can be assigned to asymmetric stretching vibrations of the PO_4 group [11].

X-ray diffraction data. Figure 3 shows the X-ray diffraction pattern of a ZTP with the Zr : Ti molar ratio of 95 : 5 as an example. As seen from this figure, the sample is partially crystalline.

Batch Adsorption Experiments

Effect of *V/m* ratio. The effect of the *V/m* ratio (60–260 mL g^{-1}) on the adsorption of $^{141}Ce(III)$, $^{160}Tb(III)$, and $^{169}Yb(III)$ from dilute HCl onto ZTP with the Zr : Ti molar ratio of 95 : 5 and particle size of 160–280 μm was studied at initial pH 2.8 ± 0.05, contact time of 24 h, and temperature of 30 ± 1°C. The results are shown in Fig. 4. As can be seen, the uptake percentage decreases with increasing *V/m* for all the lanthanides studied. The uptake percentage of ^{160}Tb is slightly higher than that of ^{141}Ce and ^{169}Yb. At lower *V/m* values, the ionic species of all the studied elements are completely adsorbed.

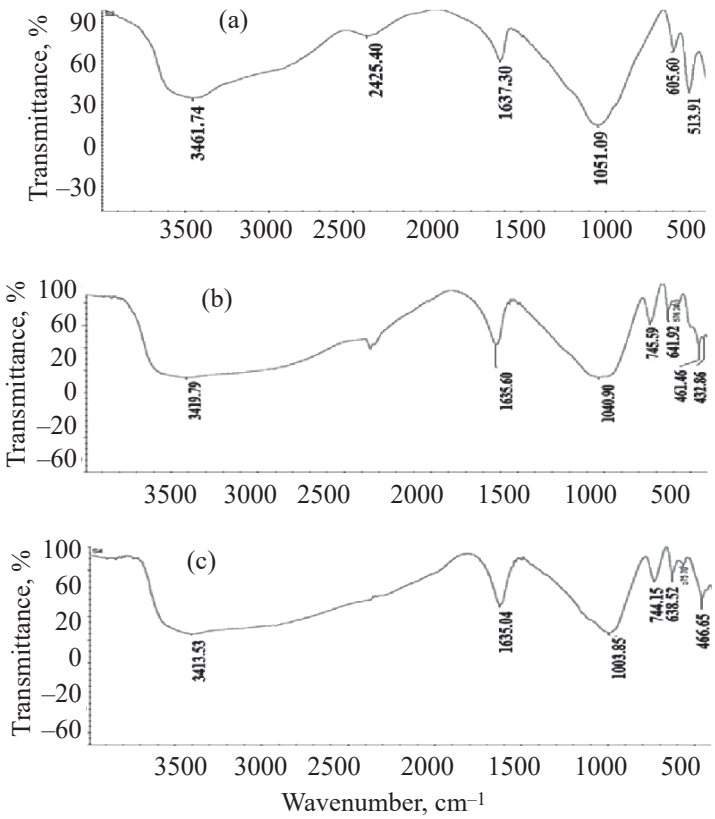

Fig. 2. FT-IR spectra of the ZTP samples. Zr : Ti molar ratio: (a) 95 : 5, (b) 25 : 75, and (c) 5 : 95.

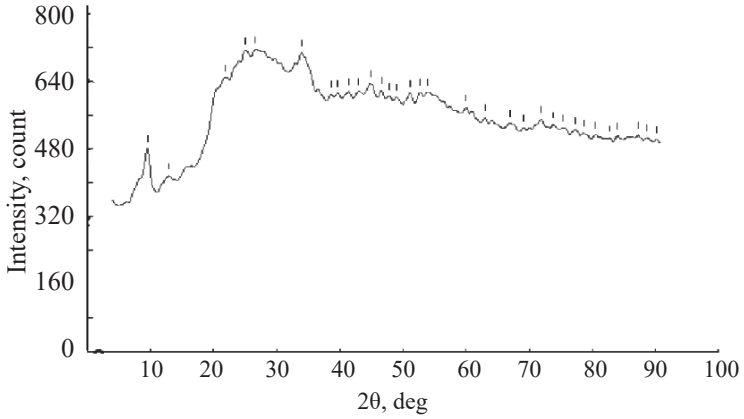

Fig. 3. X-ray diffraction pattern of the ZTP sample. Zr : Ti molar ratio 95 : 5.

Therefore, the value of V/m = 100 mL g^{-1} was chosen for further studies.

Effect of pH. The effect of initial pH (1.5–6) on the adsorption of the three lanthanide ionic species onto ZTP with the Zr : Ti molar ratios of 95 : 5 and 5 : 95 and particle size of 160–280 μm was studied at a contact time of 24 h, V/m = 100 mL g^{-1}, and 30 ± 1°C. At pH > 5.6, the trivalent lanthanide ions without complexing agents tend to hydrolyze [6]; therefore, the study was carried out at pH ≤ 5. As can be seen from Figs. 5a and 5b, the equilibrium is reached at the initial pH ≈ 2.5. The adsorption onto ZTP with the Zr: Ti molar ratio of 95 : 5 is much higher than onto ZTP with the Zr : Ti molar ratio of 5 : 95.

The increase in the adsorption with an increase in the Zr : Ti molar ratio was also observed in the previous study for the adsorption of various metal ionic species from acid solutions onto ZTP with different mole ratios [9, 10].

The uptake percentage for the adsorption onto both types of ZTP increases in the order Tb > Yb > Ce. Lanthanides form large cations (Table 2). The chemical bonding of such cations is predominantly ionic and depends on the ionic potential (Z/r), where Z is the ionic charge and r is the ionic radius [1, 12] In addition, lanthanide cations prefer O-donor ligands [1]. Cations are sorbed onto inorganic ion exchangers in a dehydrated or partially hydrated form [13], in contrast to adsorption onto organic ion exchangers where hydrated cations are adsorbed. The possible exchange sites on ZTP are the deprotonated OH groups. Ions of higher ionic potential (or higher charge) are expected to be sorbed preferentially (electroselectivity of ions). The higher percentage uptake in the case of Tb compared to Yb can be attributed to the adsorption of Tb(III) in the dehydrated form and of Yb in the partially hydrated form. Yb has smaller ionic radius; therefore, it is hydrated more strongly, which results in adsorption of partially hydrated ionic species. Table 3 represents some properties of Ce, Tb and Yb.

The adsorption is accompanied by a slight decrease in the initial pH values. This is attributed to the release of hydrogen ions of OH groups on ZTP during the exchange process. The chemical formula of ZTP may approximately be given as $Zr_{0.55}Ti_{0.45}(H_2PO_4)_2 \cdot H_2O$ [14] or $M^{IV}(HPO_4)_2 \cdot nH_2O$, where M^{IV} = Zr(IV) or Ti(IV) [15].

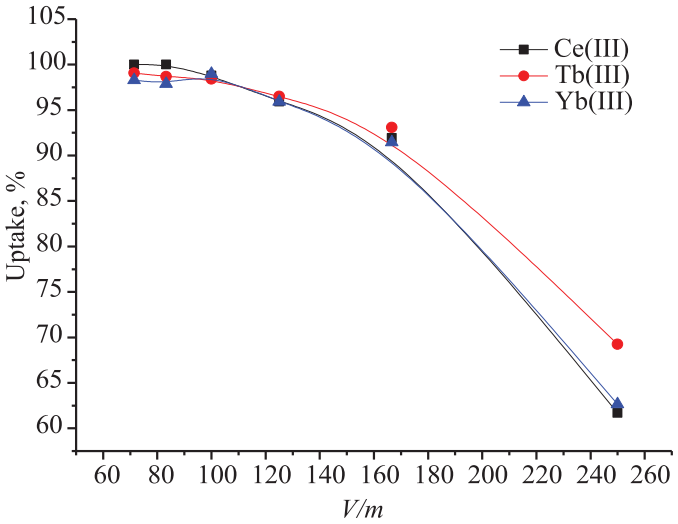

Fig. 4. (Color online) Effect of V/m ratio on the uptake of Ce(III), Tb(III), and Yb(III) by ZTP. Zr: Ti molar ratio 95 : 5, particle size 160–280 μm, 30 ± 1°C, contact time 24.0 h, pH_{init} ≈ 2.8, concentrations of Ce(III), Tb(III), and Yb(III) 1.92×10^{-4}, 2.58×10^{-5}, and 1.60×10^{-5}, respectively.

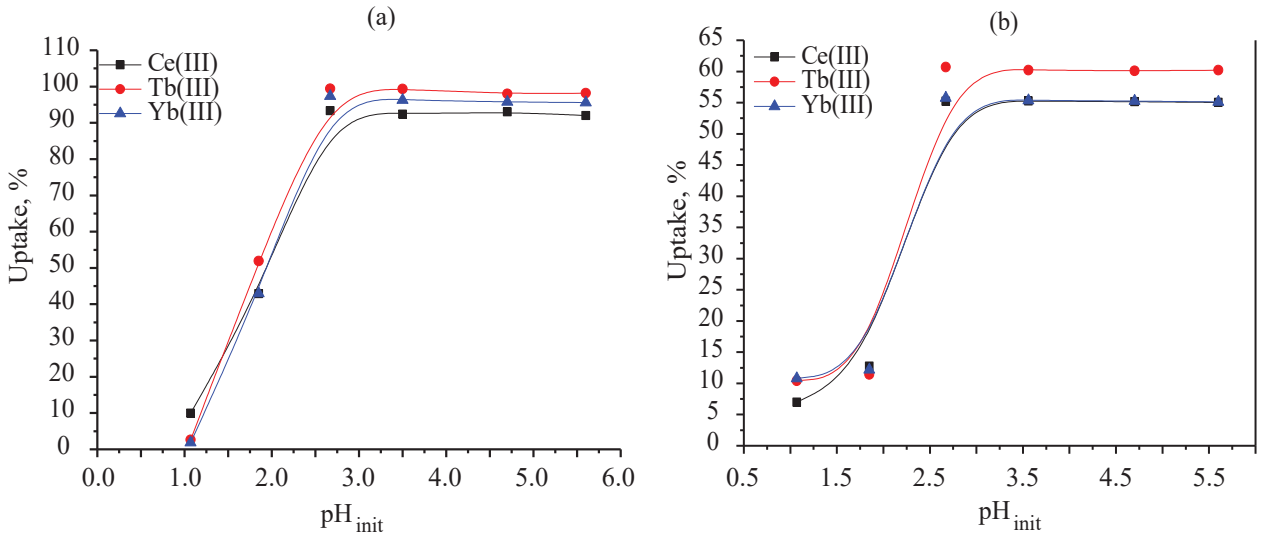

Fig. 5. (Color online) Effect of pH on the uptake of Ce(III), Tb(III), and Yb(III) on ZTP. Zr: Ti molar ratio: (a) 95 : 5 and (b) 5 : 95. Particle size 160–280 μm, 30 ± 1°C, contact time 24.0 h, V/m = 100 mL g^{-1}, and concentrations of Ce, Tb and Yb 1.28 × 10^{-4}, 1.72 × 10^{-5}, and 6 × 10^{-5} M, respectively.

The proposed chemical structure of ZTP may be schematically represented as follows:

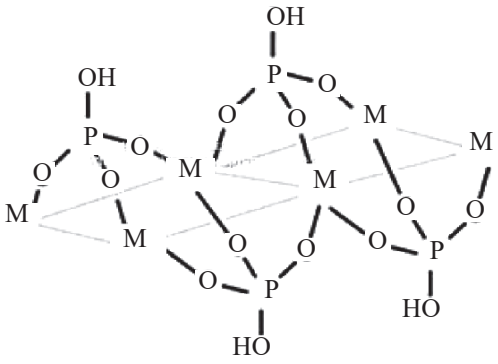

where M = Zr or Ti.

The possible exchange sites are hydroxyl groups [9], which can be deprotonated, even in acidic media, under the action of multicharged cations.

The proton exchange for a metal ion M_{aq}^{n+} in an ion exchanger R can be represented as follows:

$$M_{aq}^{n+} + \overline{nHR} \leftrightarrow nH_{aq}^{+} + MR_n,$$

where the overscore refers to the solid phase (water of hydration is omitted for simplicity). The equilibrium constant of this reaction K_H^M is given by

$$K_H^M = \frac{[H_{aq}^{+}]^n[\overline{MR_n}]}{[HR]^n[M_{aq}^{n+}]}. \quad (6)$$

Table 2. Diffusion coefficients for adsorption of Ce(III), Tb(III) and Yb(III) onto ZTP with the Zr : Ti molar ratio of 95 : 5 at 30 ± 1°C

Particle size, μm	Mean particle radius, cm	D_i × 10^{14}, m^2 s^{-1}			R^2		
		Ce(III)	Tb(III)	Yb(III)	Ce(III)	Tb(III)	Yb(III)
160	0.008	2.204	2.096	2.118	0.9996	0.998	0.9937
160–280	0.011	3.596	2.717	2.390	0.9998	0.997	0.99718
280–315	0.01487	5.0782	4.105	3.476	0.9992	0.9901	0.99653

Table 3. Thermodynamic functions for the adsorption of Ce(III), Yb(III), and Tb(III) on ZTP at different temperatures

T, K	$K_c = F_e/(1 - F_e)$			ΔG°, kJ mol^{-1}			ΔH°, kJ mol^{-1}			ΔS°, kJ mol^{-1} K^{-1}		
	Ce^{3+}	Tb^{3+}	Yb^{3+}	Ce^{3+}	Tb^{3+}	Yb^{3+}	Ce^{3+}	Tb^{3+}	Yb^{3+}	Ce^{3+}	Tb^{3+}	Yb^{3+}
295	15.69	21.47	15.67	–6.75	–7.52	–6.75	32.22	32.81	32.51	0.138	0.136	0.133
313	30.75	38	27.98	–8.91	–9.94	–9.06						
318	42.10	56.67	41.19	–9.89	–10.67	–9.83						

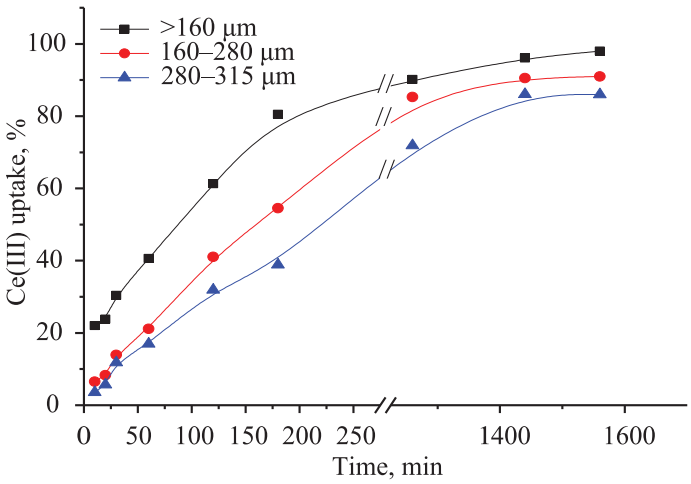

Fig. 6. (Color online) Effect of contact time on the Ce(III) uptake on ZTP. Zr : Ti molar ratio 95 : 5, 30 ± 1°C, pH_{init} 2.65 ± 0.05, V/m = 100 mL g^{-1}, Ce(III) concentration 1.28 × 10^{-4} M.

Because the metal ion concentration used is generally less than the H^+ concentration, $[HR]^n$ in Eq. (6) can be considered constant. On the other hand, the distribution coefficient K_d of the metal ion at equilibrium is given by

$$K_d = \overline{[MR_n]}[M^{n+}]. \quad (7)$$

Substituting Eq. (7) in (6), we obtain

$$K_d = K_H^M \frac{\overline{[HR]^n}}{[H_{aq}^+]^n} \frac{K}{[H_{aq}^+]^n}, \quad (8)$$

where $K = K_H^M[HR]^n$; i.e., K_d decreases with an increase in the hydrogen ion concentration.

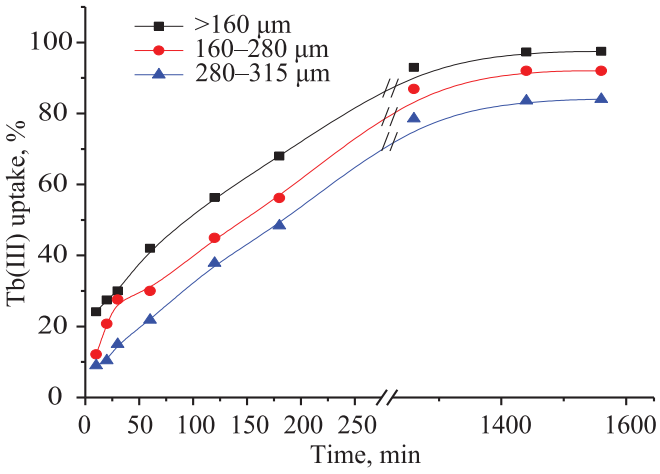

Fig. 7. (Color online) Effect of contact time on the Tb(III) uptake on ZTP. Zr : Ti molar ratio 95 : 5, 30 ± 1°C, pH_{init} 2.65 ± 0.05, V/m = 100 mL g^{-1}, Tb(III) concentration 1.72 × 10^{-5} M.

Effect of particle size. The effect of ZTP particle size on the lanthanide sorption kinetics at the Zr : Ti molar ratio 95 : 5 is illustrated in Figs. 6–8 for ^{141}Ce(III), ^{160}Tb(III), and ^{169}Yb(III), respectively. The initial pH was adjusted at 2.8 ± 0.05 to avoid the expected hydrolysis of these ions at higher pH values [6]. The adsorption kinetics is similar in all cases. The equilibrium is attained in approximately 30 h. The uptake percentage increases with decreasing particle size, suggesting the role of the diffusion process. The decrease in the particle size leads to acceleration of a process controlled by both film diffusion or diffusion in an ion exchanger particle [12], but has no effect on the chemically controlled process [13].

The effect of diffusion was analyzed using the equation for particle diffusion [16, 17]

$$F = Q_t / Q_e = 1 - 6\pi^{-2} \sum_{n=1}^{\infty} [\exp(-n^2\pi^2 D_i t^2 / r^2) / n^2] \quad (9)$$

or

$$F = Q_t / Q_e = 1 - 6\pi^{-2} \sum_{n=1}^{\infty} [\exp(-n^2\beta_t) / n^2], \quad (10)$$

where $\beta_t = \frac{\pi^2 D_i}{r^2}$.

The β_t values were calculated using an equation derived by Reichenberg [18]; Q_t and Q_e are the amounts of the adsorbed ion at time t and at equilibrium, respectively; r is the particle radius; and D_i is the

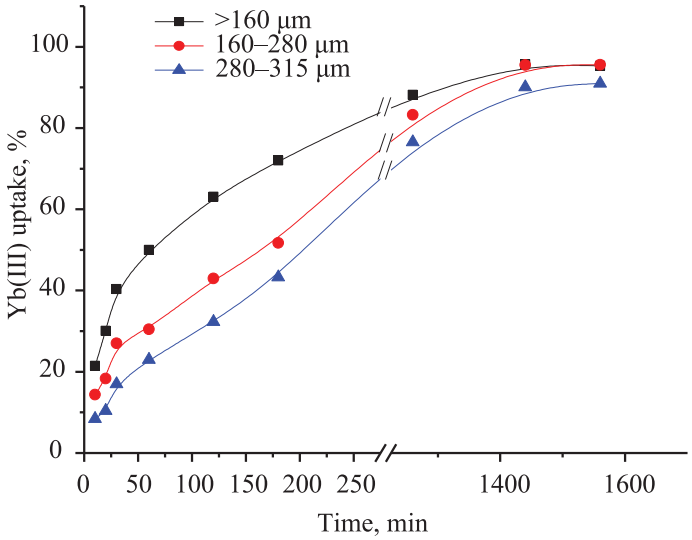

Fig. 8. (Color online) Effect of contact time on the Yb(III) uptake on ZTP. Zr : Ti molar ratio 95 : 5, 30 ± 1°C, pH_{init} 2.65 ± 0.05, V/m = 100 mL g^{-1}, Yb(III) concentration 4 × 10^{-5} M.

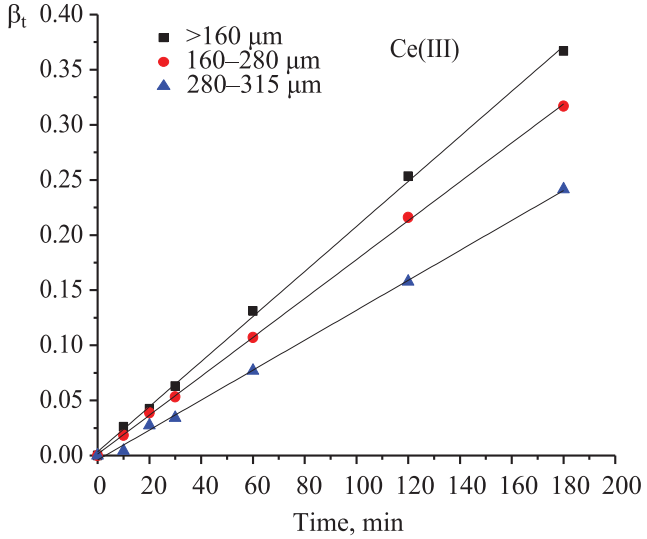

Fig. 9. (Color online) Relationship between β_t and contact time for the sorption of Ce(III) on ZTP. Zr : Ti molar ratio 95 : 5, pH_{init} 2.8 ± 0.05, 30 ± 1°C, V/m = 100 mL g^{-1}.

effective diffusion coefficient of the sorbate ion in the exchanger particle. According to Eq. (10), the plot of β_t vs. t should be a straight line passing through the origin, and D_i can be calculated from the slope of β_t. β_t is inversely proportional to the square of the particle radius. Since $F(r)$ is a function of the variable $D_i t/r^2$, the time required to attain any given degree of exchange is inversely proportional to the effective diffusion coefficient and is directly proportional to r^2.

Figures 9–11 show the relationship between β_t and t for Ce(III), Tb(III), and Yb(III) sorption, respectively, onto ZTP particles of different sizes at the Zr : Ti molar ratio of 95 : 5.

The internal diffusion coefficients D_i for Ce(III), Tb(III), and Yb(III) in ZTP with the Zr : Ti molar ratio of 95 : 5 and various particle sizes were determined from the slopes of the straight lines in Figs. 9–11 and are given in Table 3.

Effect of sorbate concentration: The effect of the metal ion concentration on the adsorption of ^{141}Ce(III), ^{160}Tb(III), and ^{169}Yb(III) onto ZTP with the Zr : Ti mole ratio of 95 : 5 was studied at initial pH 2.6 ± 0.05, particle size of 160–280 μm, temperature of 30 ± 1°C, and V/m = 100 mL g^{-1}. The concentrations were varied in the ranges 8.36 × 10^{-6}–8.38 × 10^{-5} M) for Ce(III), 7.31 × 10^{-6}–7.31 × 10^{-5} M for ^{160}Tb, and 1.3 × 10^{-5}–1.33 × 10^{-3} M for ^{169}Yb(III). As can be seen, the uptake percentage decreases with an increase in the adsorbate concentration in all the cases. At short contact time, the adsorbate concentration does not influence K_d. This indicates that the process rate is not controlled by film diffusion.

Effect of temperature. The adsorption of Ce(III), Tb(III), and Yb(III) onto ZTP with the Zr : Ti molar ratio of 95 : 5 and particle size of 160–280 μm was studied at initial pH 2.6 ± 0.05 and various temperatures: 22, 40, and 45°C. The results are shown in Figs. 12–14.

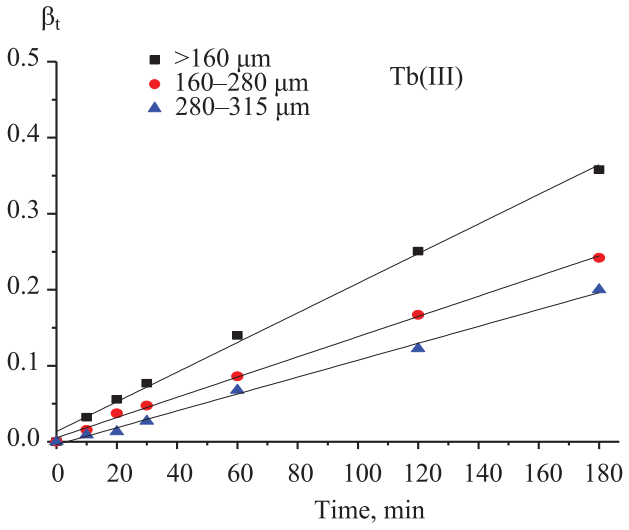

Fig. 10. (Color online) Relationship between β_t and contact time for the sorption of Tb(III) on ZTP. Zr : Ti molar ratio 95 : 5, pH_{init} 2.8 ± 0.05, 30 ± 1°C, V/m = 100 mL g^{-1}.

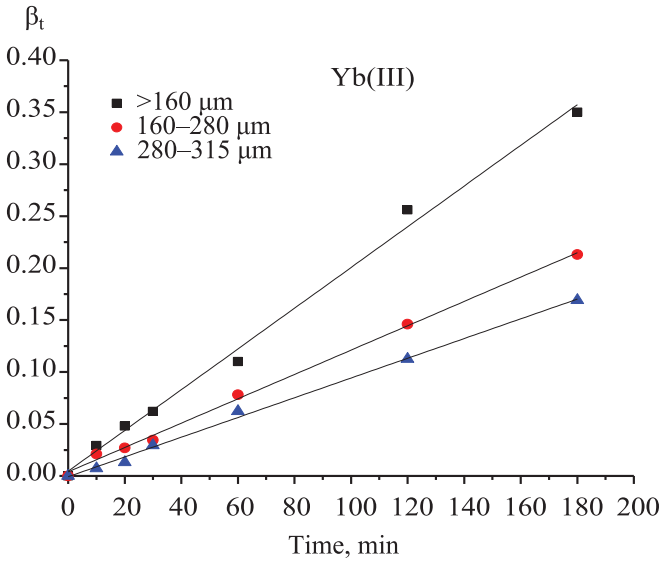

Fig. 11. (Color online) Relationship between β_t and contact time for the sorption of Yb(III) on ZTP. Zr : Ti molar ratio 95 : 5, pH_{init} 2.8 ± 0.05, 30 ± 1°C, V/m = 100 mL g^{-1}.

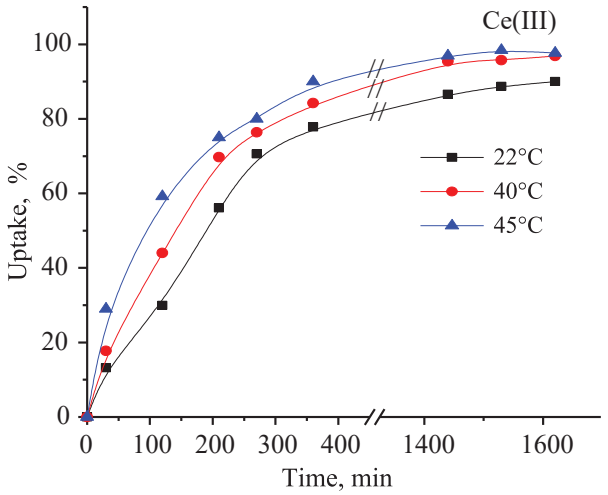

Fig. 12. (Color online) Effect of contact time on the Ce(III) uptake on ZTP. Zr: Ti molar ratio 95 : 5, particle size 160–280 μm, V/m = 100 mL g^{-1}, Ce(III) concentration 1.92 × 10^{-4} M.

As can be seen, the uptake percentage increases with temperature. The metal ion fractions adsorbed onto ZTP and their corresponding distribution coefficients were calculated at different temperatures using Eqs. (3) and (4). The free energy of the adsorption is given by the Gibbs equation [19]:

$$\Delta G^{\circ} = -RT\ln K_c, \quad (11)$$

where K_c is the adsorption equilibrium constant, R is the molar gas constant, and T is the absolute temperature (K). The sorption equilibrium constant (K_c) is calculated using the following equation:

$$K_c = F_e/(1 - F_e), \quad (12)$$

where F_e is the fraction of the metal ion adsorbed at equilibrium. The results are given in Table 4.

An increase in the adsorption with temperature suggests enhancement of the adsorbate–adsorbent interactions. It also indicates that these ions undergo considerable dehydration at higher temperatures to form species of smaller size with higher K_c. The negative values of $\Delta G°$ confirm the feasibility and spontaneous nature of the sorption process. The effect of temperature is more pronounced at short contact time than at longer contact time, except for Ce(III).

The Gibbs free energy is related to the enthalpy change ($\Delta H°$) and entropy change ($\Delta S°$) by the following equation:

$$\Delta G° = \Delta H° - T\Delta S°. \quad (13)$$

These values are calculated from the slope and intercept of the plot of $\Delta G°$ vs. T (Fig. 15).

Adsorption isotherms. Two commonly used isotherm models, Langmuir and Freundlich, were applied to analyze the sorption equilibria for Tb(III) chosen as an example. ZTP with the Zr : Ti molar ratio of 25 : 75 and particle size of 160–280 μm was taken.

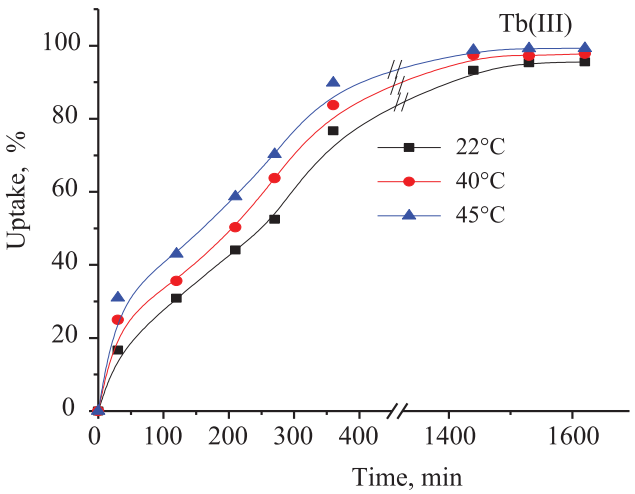

Fig. 13. (Color online) Effect of contact time on the Tb(III) uptake on ZTP. Zr: Ti molar ratio 95 : 5, particle size 160–280 μm, V/m = 100 mL g^{-1}, Tb(III) concentration 2.58 × 10^{-5} M.

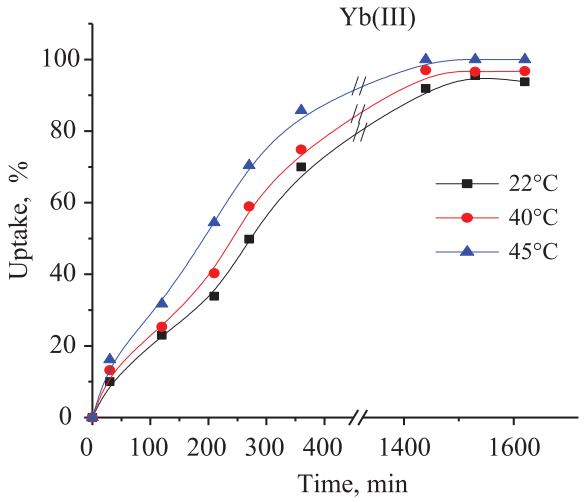

Fig. 14. (Color online) Effect of contact time on the Yb(III) uptake on ZTP. Zr: Ti molar ratio 95 : 5, particle size 160–280 μm, V/m = 100 mL g^{-1}, Yb(III) concentration 6×10^{-5} M.

Table 4. Langmuir and Freundlich isotherm parameters for the adsorption of Tb(III) onto ZTP. Zr : Ti molar ratio 25 : 75)

Langmuir model				Freundlich model		
q_{max}, mg g^{-1}	K_L	R_L	R^2	K_f	$1/n$	R^2
10.02	0.0061	0.14–0.67	0.981	0.4285	0.4558	0.8360

Table 5. Adsorption kinetics parameters for the adsorption of Ce(III), Tb(III), and Yb(III) from aqueous solutions onto ZTP

Ion	Pseudo-first-order			Pseudo-second-order		
	K_1, min^{-1}	q_e, mg g^{-1}	R^2	K_2, g mg^{-1} min^{-1}	q_e, mg g^{-1}	R^2
Ce(III)	0.0846	4.7731	0.970	5.127×10^{-6}	132.1004	0.992
Tb(III)	0.0054	0.638	0.988	0.00169	3.977725	0.999
Yb(III)	0.0065	1.486	0.970	2.265×10^{-5}	47.16981	0.993

The linear form of the Langmuir isotherm is given by the following equation [20, 21]:

$$\frac{C_e}{q_e} = \frac{1}{K_L q_{max}} + \frac{C_e}{q_{max}}, \quad (14)$$

where C_e (mg L^{-1}) is the equilibrium concentration of adsorbate in the solution, q_e (mg g^{-1}) is the amount of the adsorbate adsorbed per unit mass of the adsorbent, q_{max} (mg g^{-1}) is the theoretical maximum sorption capacity, and K_L (L mg^{-1}) is the Langmuir sorption constant related to the adsorption energy. q_{max} and K_L were calculated from the slope and intercept of linear plots of C_e/q_e vs. C_e (Fig. 16). The separation factor (R_L) was calculated as follows [20]:

$$R_L = \frac{1}{1 + K_L C_0}, \quad (15)$$

where C_0 is initial adsorbate concentration (mg L^{-1}).

The logarithmic form of the Freundlich isotherm model can be expressed as follows [20, 22]:

$$\log q_e = \log K_f + \frac{1}{n} \log C_e, \quad (16)$$

where C_e (mg L^{-1}) is the equilibrium adsorbate concentration in the solution, q_e (mg g^{-1}) is the amount of the adsorbate adsorbed per unit mass of the adsorbent, K_f and are Freundlich constants, K_f is the adsorption capacity of the adsorbent, and n is an indicator for

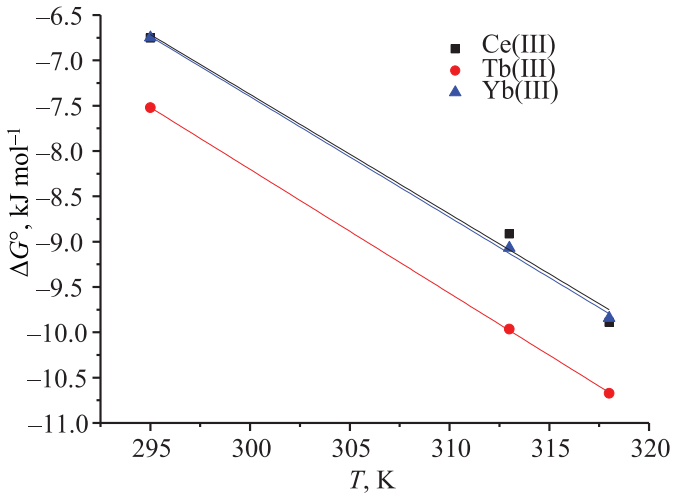

Fig. 15. (Color online) Relationship between the Gibbs free energy change and temperature for the sorption of Ce(III), Tb(III), and Yb(III) onto ZTP. Zr : Ti molar ratio 95 : 5, particle size 160–280 μm.

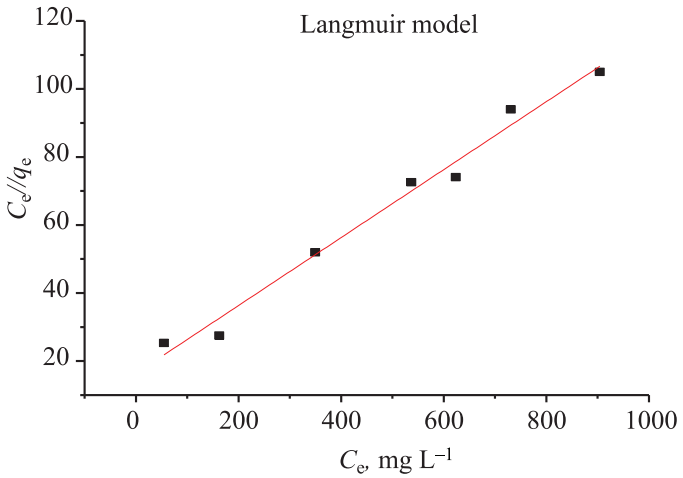

Fig. 16. (Color online) Langmuir isotherm for the adsorption of Tb(III) onto ZTP. Zr : Ti molar ratio 25 : 75, particle size 160–280 μm, contact time 24 h, pH_{init} 2.8 ± 0.05, 26 ± 1°C, V/m = 100 mL g^{-1}.

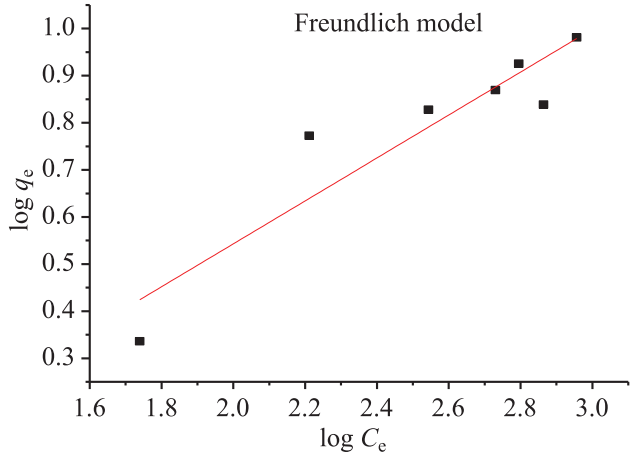

Fig. 17. (Color online) Freundlich isotherm for the adsorption of Tb(III) onto ZTP. Zr : Ti molar ratio 25 : 75, particle size 160–280 μm, contact time 24 h, pH_{init} 2.8 ± 0.05, 26 ± 1°C, V/m = 100 mL g^{-1}.

favorable or unfavorable adsorption process. K_f and n are the Freundlich constants and are calculated from the intercept and slope of the relationship between log q_e and log C_e. Figure 17 shows these data. The n value demonstrates the favorability of the adsorption process ($1/n < 1$ corresponds to favorable adsorption, and $1/n > 1$, to cooperative adsorption). The high correlation coefficients R^2 (Table 5) indicate that the experimental data for the adsorption of Tb(III) follow the Langmuir model better than the Freundlich model.

Adsorption kinetics. Pseudo-first-order and pseudo-second-order models were applied to investigate the kinetics of the adsorption of Ce(III), Tb(III), and Yb(III) onto ZTP with the Zr : Ti molar ratio of 95 : 5.

The pseudo-first-order model is described by the following equation [19, 22]:

$$\ln(q_e - q_t) = \ln q_e + K_1 t, \quad (17)$$

where q_e is the amount of the metal ion adsorbed onto the adsorbent at equilibrium (mg g^{-1}), q_t is the amount of the metal ion adsorbed at a given time, t is the adsorption time, and K_1 is the rate constant (min^{-1}). The slopes and intercepts of plots of ln ($q_e - q_t$) vs. time were calculated to determine the first-order rate constant K_1. Figure 18 shows these data.

The pseudo-second-order model is described by the following linear equation [19, 22]:

$$\frac{t}{q_t} = \frac{1}{K_2 q_e^2} + \frac{1}{q_e} t, \quad (18)$$

where K_2 is the pseudo-second-order rate constant (g mg^{-1} min^{-1}). The values of q_e and K_2 were determined from the slope and intercept of the plots of t/q_t vs. t. Figure 19 shows these data.

The pseudo-second-order model fits sorption data better than the pseudo-first-order model does (Table 5). The correlation coefficients (R^2) for the linear plots of

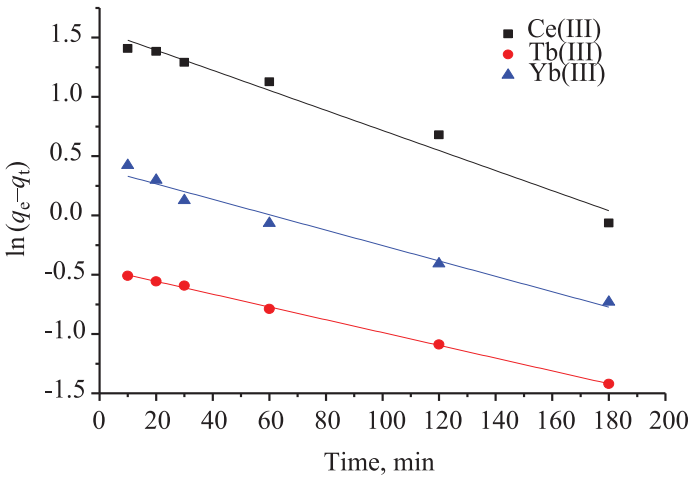

Fig. 18. (Color online) Pseudo-first-order kinetic plots for the sorption of Ce(III), Tb(III), and Yb(III) from aqueous solutions onto ZTP. Zr : Ti molar ratio 95 : 5, particle size >160 μm, 30 ± 1°C, pH_{init} 2.65 ± 0.05, V/m = 100 mL g^{-1}.

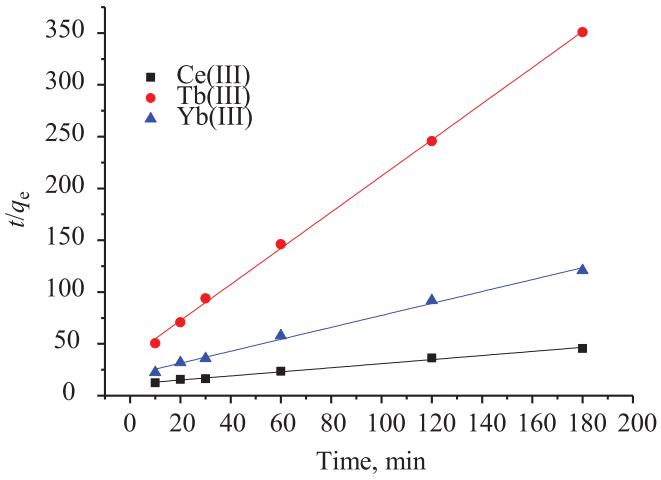

Fig. 19. (Color online) Pseudo-second-order kinetic plots for the sorption of Ce(III), Tb(III), and Yb(III) from aqueous solutions onto ZTP. Zr : Ti molar ratio 95 : 5, particle size >160 μm, 30 ± 1 °C, pH_{init} 2.65 ± 0.05, V/m = 100 mL g^{-1}.

t/q_t vs. t in the pseudo-second-order model are higher than 0.99.

CONCLUSIONS

Samples of zirconium titanium phosphate ion exchanger were synthesized at different Zr : Ti molar ratios. These samples were characterized using FT-IR, XRD, SEM, and pore size analyhsis. The samples efficiently adsorb Ce(III), Tb(III), and Yb(III) ionic species from dilute HCl solutions. Complete adsorption from aqueous solutions was achieved under certain conditions.

The adsorption is controlled by particle diffusion in each case. The calculated diffusion coefficients of all the lanthanide ions studied are of the order of 10^{-14} m^2 s^{-1}, suggesting the chemisorption nature of the process. The uptake percentage decreases in the order Tb > Yb > Ce. This result suggests the adsorption of Yb as partially hydrated ions in contrast to Tb and Ce adsorbed in the dehydrated form. The thermodynamic functions $\Delta G°$, $\Delta H°$, and $\Delta S°$ of the sorption reaction were calculated. The adsorption was found to follow the Langmuir isotherm better than th Freundlich isotherm. The adsorption follows a pseudo-second-order model.

CONFLICT OF INTEREST

The authors state that they have no conflict of interest.

REFERENCES

1. Greenwood, N.N. and Earnsha, W.A., *Chemistry of the Elements,* Oxford: Butterworth, 1997.
2. *British Geological Survey 2010, Rare Earth Elements.* http:/www.minerals.uk.com
3. Gupta, C.K. and Krishnamurthy, N., *Extractive Metallurgy of Rare Earths,* New York: CRC, 2005.
4. Kim, E. and Osseo-Asare, K., *Hydrometallurgy,* 2012, vols. 113–114, p. 67.
5. Moller, T., *Comprehensive Inorganic Chemistry, vol. 4: Lanthanides,* Bailar, J.C., Emeleus, H.J., Nyholm, R., and Trotman-Dickenson, A.F., Eds., New York: John Wiley and Sons Inc., 1975.
6. Schweitzer, G.K. and Pesterfield, L.L., *The Aqueous Chemistry of the Elements,* New York: Oxford Univ. Press, 2010.
7. Seelmann-Eggebert, W., Pfennig, G., and Münzel, H., *Chart of the Nuclides,* Germany: KFK, 1991.
8. Marei, S.A. and Shakshooki, S.K., *Radiochim. Radioanal. Lett.,* 1972, vol. 4, p. 187.
9. El-Sweify, F.H., Eldin, A.K., Abd Elmonem, D., Adel, N., and Hegazy, W.S., *Arab J. Nucl. Sci. Appl.,* 2013, vol. 46, no. 4, p. 62.
10. El-Sweify, F.H., El-Shazly, E.A.A., and Salama, Sh.M., *Radiochim. Acta,* 2018, vol. 406, no. 3, p. 207.
11. Colthup, N.B., Daly, L.H., and Stephen, E.W., *Introduction to Infrared and Raman Spectroscopy,* Weinheim: Academic Press, 1965.
12. Clearfield, A., *Inorganic Ion Exchange Materials,* Boca Raton: CRC, 1982.
13. Reichenberg, D., *Selectivity of Ion Exchange: A Series of Advances,* Marinsky, J.A. and Marcus, Y., Eds., New York: Dekker, 1965.
14. Thakkar, R. and Chudasama, U., *J. Hazard. Mater.,* 2009, vol. 172, p. 129.
15. Rakesh, P.T. and Uma, V.C., *Coll. Czech. Chem. Commun.,* 2007, vol. 72, no. 9, p. 1306.
16. Boyd, G.E., Adamson, A.W., and Myers, L.S., *J. Am. Chem. Soc.,* 1947, vol. 69, p. 2836.
17. El-Sweify, F.H., Abdel Fattah, A.A., El-Sheikh, R., Aly, S.M., and Ghamry, M.A., *Radiochemistry,* 2018, vol. 60, no. 3, p. 274. https://doi.org/10.1134/S1066362218030086
18. Reichenberg, D., *J. Am. Chem. Soc.,* 1953, vol. 75, p. 589.
19. El-Kamash, A.M., El-Gammal, B., and El-Sayed, A.A., *J. Hazard. Mater.,* 2007, vol. 141, p. 719.
20. Foo, K.Y. and Hameed, B.H., *Chem. Eng. J.,* 2010, vol. 156, p. 2.
21. Rainert, K.T., Nunes, H.C.A., Gonçalves, M.J., and Tavares, L.B.B., *Desalin. Water Treat.,* 2017, vol. 86, p. 203.
22. Abdelmonem, I.M., Metwally, E., Siyam, T.E., Abou El-Nour, F., and Mousa, A.M., *J. Radioanal. Nucl. Chem.,* 2019, vol. 319, p. 1145. https://doi.org/10.1007/s10967-018-6392-1